Journal of Systems Engineering and Electronics
Vol. 31, No. 5, October 2020, pp.939 – 949

Moving target localization for multistatic passive radar using delay, Doppler and Doppler rate measurements

ZHAO Yongsheng, HU Dexiu*, ZHAO Yongjun, and LIU Zhixin

Data and Target Engineering Institute, PLA Strategic Support Force Information Engineering University, Zhengzhou 450001, China

Abstract: Time delay and Doppler shift between the echo signal and the reference signal are two most commonly used measurements in target localization for the passive radar. Doppler rate, which can be obtained from the extended cross ambiguity function, offers an opportunity to further enhance the localization accuracy. This paper considers using the measurement Doppler rate in addition to measurements of time delay and Doppler shift to locate a moving target. A closed-form solution is developed to accurately and efficiently estimate the target position and velocity. The proposed solution establishes a pseudolinear set of equations by introducing some additional variables, imposes weighted least squares formulation to yield a rough estimate, and utilizes the function relation among the target location parameters and additional variables to improve the estimation accuracy. Theoretical covariance and Cramer-Rao lower bound (CRLB) are derived and compared, analytically indicating that the proposed solution attains the CRLB. Numerical simulations corroborate this analysis and demonstrate that the proposed solution outperforms existing methods.

Keywords: target localization, multistatic passive radar, time delay, Doppler shift, Doppler rate.

DOI: 10.23919/JSEE.2020.000071

1. Introduction

Multistatic passive radar (MPR), which employs ambient signals (FM radio [1 – 3], digital TV [4 – 6], digital audio broadcast [7 – 9], cellphone basestation [10 – 13], WiMax [14,15], WiFi [16 – 18], satellite [19 – 21], non-cooperative radar signal [22], etc.) as the transmitters to detect and locate potential targets, is an attractive system for surveillance purposes. Owing to its distinct merits, such as covert operation, wide coverage, small size and hence easy to deploy, low costs of operation and maintenance, immune to directional interference, capabilities against stealth aircraft, etc., MPR has been studied for several decades and is still a hot area of research [23,24].

The receiver of passive radar usually deploys two receiving channels: the reference channel and the echo channel [25]. The reference channel, which can be implemented as a directional antenna or a digitally formed beam, points towards the transmitter to receive the original transmitted signal, i.e., the direct path signal. The echo channel looks towards the area of interest to collect echo signals from potential targets [26]. The echo signal is usually much weaker in power, hence coherent integration is needed to improve the signal-to-noise ratio (SNR) [27]. One of the most typical coherent integration methods is the cross ambiguity function (CAF) [28], from which time delay and Doppler shift between the echo signal and the reference signal can be acquired by locating the correlation peak. Time delay and Doppler shift are two most commonly used measurements to estimate the target position and velocity, and copious localization methods are developed based on these two measurements [29 – 32].

The CAF method works well in most of the cases. However, in some situations, such as detection and localization of manoeuvring targets, the simplified assumptions made in the derivation of the CAF lead to suboptimal performance. Another situation where more complicated signal processing is required is when long time coherent integration (of the order of 1 s) is desired. For this purpose, recently some novel coherent integration methods [33 – 35], such as the modified CAF [34], are proposed, from which time delay, Doppler shift and Doppler rate can be obtained simultaneously. In source localization problem, the Doppler rate measurement has been used in addition to time delay and Doppler shift measurements to improve the localization accuracy [36,37]. Inspired by this, for moving target localization in the multistatic passive radar, we hopefully determine the target position and velocity with a higher accuracy by jointly using the Doppler rate measurements. However, despite the fine prospects, up to now there does not exist any publication in the open literature that ad-

Manuscript received March 18, 2019.
*Corresponding author.
This work was supported by the National Natural Science Foundation of China (61703433).

dresses combining measurements of time delay, Doppler shift and Doppler rate to estimate the target position and velocity in the multistatic passive radar.

Extracting the target position and velocity from measurements of time delay, Doppler shift and Doppler rate acquired at a single observation is a crucial and challenging operation, on account of the extreme nonlinearity implied in the measurement equations. Exhaustive search in the solution space seems to be a basic alternative to tackle the nonlinearity. Nevertheless, this technique usually endures a heavy computational burden because of the high dimensionality, which prohibits real-time implementation. Iterative approaches, such as Taylor series approach, Newton-Raphson approach and expectation-maximization approach, therefore, have to be envisaged, to achieve desirably accurate results with an acceptable complexity. However, iterative approaches are known to converge to the global optimal solution only if the initial solution guess is close enough to the true values of parameters. Otherwise, they may converge to a local optimum or even diverge. Therefore, there is yet a need for an alternative solution method that requires no initial guess.

Closed-form solutions are always compelling to researchers due to their advantages of independence on initial guess and acceptable computational complexity. Motivated by this, we derive in this paper a closed-from solution for moving target localization using measurements of time delay, Doppler shift and Doppler rate in the multistatic passive radar. The proposed solution follows the basic idea of two-step weighted least squares (WLS) [38], and further extends our previous work in [32] that determines the target position and velocity only using measurements of time delay and Doppler shift. It is generally composed of two WLS steps. In the first WLS step, by introducing some extra additional variables, the proposed solution first translates the time delay, Doppler shift and Doppler rate equations to a set of linear equations, from which a rough estimate of target location and additional variables is obtained by using WLS minimization. Next, in the second WLS step, by using the functional relation between the additional variables and target location, we extract another set of linear equations, from which a refined estimate of target location is finally obtained by using WLS minimization again. To the best of our knowledge, the proposed solution is the first localization method jointly by using measurements of time delay, Doppler shift and Doppler rate in the multistatic passive radar literature. Theoretical error analysis and numerical simulations are performed and verify the validity and efficiency of the proposed solution.

The remaining sections of this paper are organized as follows. In Section 2, we present the measurement model and the target localization problem. In Section 3, the proposed closed-form solution for the target position and velocity is given. In Section 4, we analyze the bias, covariance as well as the Cramér-Rao lower bound (CRLB). In Section 5, the performance of the proposed solution is evaluated via several numerical examples. Finally, in Section 6, we make some concluding remarks.

2. Problem formulation

In general, as illustrated in Fig. 1, an MPR system with M transmitters and N receivers is deployed to locate a moving target with an unknown position $\boldsymbol{u} = [x, y, z]^{\mathrm{T}}$ and velocity $\dot{\boldsymbol{u}} = [\dot{x}, \dot{y}, \dot{z}]^{\mathrm{T}}$. The position and the velocity of the mth transmitter are known and denoted by $\boldsymbol{s}_m^t = [x_m^t, y_m^t, z_m^t]^{\mathrm{T}}$ and $\dot{\boldsymbol{s}}_m^t = [\dot{x}_m^t, \dot{y}_m^t, \dot{z}_m^t]^{\mathrm{T}}$, and the position and the velocity of the nth receiver are known and denoted by $\boldsymbol{s}_n^r = [x_n^r, y_n^r, z_n^r]^{\mathrm{T}}$ and $\dot{\boldsymbol{s}}_n^r = [\dot{x}_n^r, \dot{y}_n^r, \dot{z}_n^r]^{\mathrm{T}}$.

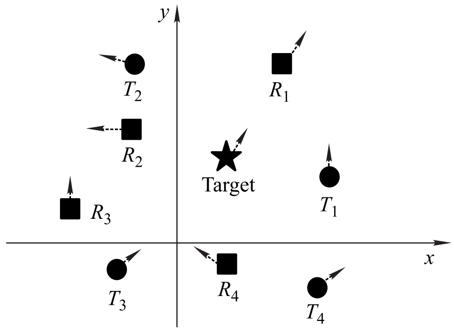

Fig. 1 Localization geometry

Using the above notations, the range, rate and acceleration between the mth transmitter and the target are respectively expressed as

$$R_m^t = \|\boldsymbol{u} - \boldsymbol{s}_m^t\|, \tag{1}$$

$$\dot{R}_m^t = \frac{(\boldsymbol{u} - \boldsymbol{s}_m^t)^{\mathrm{T}}(\dot{\boldsymbol{u}} - \dot{\boldsymbol{s}}_m^t)}{R_m^t}, \tag{2}$$

$$\ddot{R}_m^t = \frac{(\dot{\boldsymbol{u}} - \dot{\boldsymbol{s}}_m^t)^{\mathrm{T}}(\dot{\boldsymbol{u}} - \dot{\boldsymbol{s}}_m^t) - (\dot{R}_m^t)^2}{R_m^t}. \tag{3}$$

Likewise, the range, rate and acceleration between the target and the nth receiver are respectively stated as

$$R_n^r = \|\boldsymbol{u} - \boldsymbol{s}_n^r\|, \tag{4}$$

$$\dot{R}_n^r = \frac{(\boldsymbol{u} - \boldsymbol{s}_n^r)^{\mathrm{T}}(\dot{\boldsymbol{u}} - \dot{\boldsymbol{s}}_n^r)}{R_n^r}, \tag{5}$$

$$\ddot{R}_n^r = \frac{(\dot{\boldsymbol{u}} - \dot{\boldsymbol{s}}_n^r)^{\mathrm{T}}(\dot{\boldsymbol{u}} - \dot{\boldsymbol{s}}_n^r) - (\dot{R}_n^r)^2}{R_n^r}. \tag{6}$$

Subsequently, as defined in [34], the bistatic range, bistatic velocity and bistatic acceleration subject to the mth transmitter and the nth receiver, are respectively described by

$$r_{m,n}^o = R_m^t + R_n^r, \tag{7}$$

$$\dot{r}_{m,n}^o = \dot{R}_m^t + \dot{R}_n^r, \tag{8}$$

$$\ddot{r}_{m,n}^o = \ddot{R}_m^t + \ddot{R}_n^r. \tag{9}$$

In the presence of the additive noise, the observed bistatic range, bistatic velocity and bistatic acceleration, which are directly converted from measurements of time delay, Doppler shift and Doppler rate respectively, can be stated as

$$r_{m,n} = r^o_{m,n} + \Delta r_{m,n}, \tag{10}$$

$$\dot{r}_{m,n} = \dot{r}^o_{m,n} + \Delta \dot{r}_{m,n}, \tag{11}$$

$$\ddot{r}_{m,n} = \ddot{r}^o_{m,n} + \Delta \ddot{r}_{m,n} \tag{12}$$

where $\Delta r_{m,n}$, $\Delta \dot{r}_{m,n}$ and $\Delta \ddot{r}_{m,n}$ are the measurement noises of bistatic range, bistatic velocity and bistatic acceleration, respectively.

Next, by defining the following vector notations:

$$\boldsymbol{r} = [\boldsymbol{r}_1^{\mathrm{T}}, \boldsymbol{r}_2^{\mathrm{T}}, \dots, \boldsymbol{r}_M^{\mathrm{T}}]^{\mathrm{T}}, \boldsymbol{r}_m = [r_{m,1}, r_{m,2}, \dots, r_{m,N}]^{\mathrm{T}},$$

$$\dot{\boldsymbol{r}} = [\dot{\boldsymbol{r}}_1^{\mathrm{T}}, \dot{\boldsymbol{r}}_2^{\mathrm{T}}, \dots, \dot{\boldsymbol{r}}_M^{\mathrm{T}}]^{\mathrm{T}}, \dot{\boldsymbol{r}}_m = [\dot{r}_{m,1}, \dot{r}_{m,2}, \dots, \dot{r}_{m,N}]^{\mathrm{T}},$$

$$\ddot{\boldsymbol{r}} = [\ddot{\boldsymbol{r}}_1^{\mathrm{T}}, \ddot{\boldsymbol{r}}_2^{\mathrm{T}}, \dots, \ddot{\boldsymbol{r}}_M^{\mathrm{T}}]^{\mathrm{T}}, \ddot{\boldsymbol{r}}_m = [\ddot{r}_{m,1}, \ddot{r}_{m,2}, \dots, \ddot{r}_{m,N}]^{\mathrm{T}},$$

$$\boldsymbol{r}^o = [(\boldsymbol{r}_1^o)^{\mathrm{T}}, \dots, (\boldsymbol{r}_M^o)^{\mathrm{T}}]^{\mathrm{T}}, \boldsymbol{r}_m^o = [r^o_{m,1}, \dots, r^o_{m,N}]^{\mathrm{T}},$$

$$\dot{\boldsymbol{r}}^o = [(\dot{\boldsymbol{r}}_1^o)^{\mathrm{T}}, \dots, (\dot{\boldsymbol{r}}_M^o)^{\mathrm{T}}]^{\mathrm{T}}, \dot{\boldsymbol{r}}_m^o = [\dot{r}^o_{m,1}, \dots, \dot{r}^o_{m,N}]^{\mathrm{T}},$$

$$\ddot{\boldsymbol{r}}^o = [(\ddot{\boldsymbol{r}}_1^o)^{\mathrm{T}}, \dots, (\ddot{\boldsymbol{r}}_M^o)^{\mathrm{T}}]^{\mathrm{T}}, \ddot{\boldsymbol{r}}_m^o = [\ddot{r}^o_{m,1}, \dots, \ddot{r}^o_{m,N}]^{\mathrm{T}},$$

the bistatic range, bistatic velocity and bistatic acceleration subject to the M transmitters and N receivers, can be compactly described by

$$\boldsymbol{r} = \boldsymbol{r}^o + \Delta \boldsymbol{r}, \tag{13}$$

$$\dot{\boldsymbol{r}} = \dot{\boldsymbol{r}}^o + \Delta \dot{\boldsymbol{r}}, \tag{14}$$

$$\ddot{\boldsymbol{r}} = \ddot{\boldsymbol{r}}^o + \Delta \ddot{\boldsymbol{r}} \tag{15}$$

where

$$\Delta\boldsymbol{r} = [\Delta\boldsymbol{r}_1^{\mathrm{T}}, \dots, \Delta\boldsymbol{r}_M^{\mathrm{T}}]^{\mathrm{T}}, \Delta\boldsymbol{r}_m = [\Delta r_{m,1}, \dots, \Delta r_{m,N}]^{\mathrm{T}},$$

$$\Delta\dot{\boldsymbol{r}} = [\Delta\dot{\boldsymbol{r}}_1^{\mathrm{T}}, \dots, \Delta\dot{\boldsymbol{r}}_M^{\mathrm{T}}]^{\mathrm{T}}, \Delta\dot{\boldsymbol{r}}_m = [\Delta \dot{r}_{m,1}, \dots, \Delta \dot{r}_{m,N}]^{\mathrm{T}},$$

$$\Delta\ddot{\boldsymbol{r}} = [\Delta\ddot{\boldsymbol{r}}_1^{\mathrm{T}}, \dots, \Delta\ddot{\boldsymbol{r}}_M^{\mathrm{T}}]^{\mathrm{T}}, \Delta\ddot{\boldsymbol{r}}_m = [\Delta \ddot{r}_{m,1}, \dots, \Delta \ddot{r}_{m,N}]^{\mathrm{T}}.$$

Putting the three sets of measurements together forms the total measurement vector $\boldsymbol{\alpha} = [\boldsymbol{r}^{\mathrm{T}}, \dot{\boldsymbol{r}}^{\mathrm{T}}, \ddot{\boldsymbol{r}}^{\mathrm{T}}]^{\mathrm{T}}$. Then, the corresponding true value of the measurement vector is denoted by $\boldsymbol{\alpha}^o = [(\boldsymbol{r}^o)^{\mathrm{T}}, (\dot{\boldsymbol{r}}^o)^{\mathrm{T}}, (\ddot{\boldsymbol{r}}^o)^{\mathrm{T}}]^{\mathrm{T}}$, and the noise vector is denoted by $\Delta\boldsymbol{\alpha} = [\Delta\boldsymbol{r}^{\mathrm{T}}, \Delta\dot{\boldsymbol{r}}^{\mathrm{T}}, \Delta\ddot{\boldsymbol{r}}^{\mathrm{T}}]^{\mathrm{T}}$, which follows the Gaussian distribution with the mean zero and the covariance

$$\mathrm{E}\{\Delta\boldsymbol{\alpha}\Delta\boldsymbol{\alpha}^{\mathrm{T}}\} = \boldsymbol{Q}. \tag{16}$$

Given M transmitters and N receivers, there are MN bistatic range measurements, MN bistatic velocity measurements, and MN bistatic acceleration measurements. Now, the problem can be stated as, given the observations $\boldsymbol{\alpha}$, find the target position $\boldsymbol{u}$ and velocity $\dot{\boldsymbol{u}}$ accurately. Nevertheless, despite a clear appeal, determining the target position $\boldsymbol{u}$ and velocity $\dot{\boldsymbol{u}}$ from the observations $\boldsymbol{\alpha}$ is not tractable, since the target location parameters are nonlinearly related to the observations.

3. The proposed localization method

In this section, borrowing the basic framework of two-step WLS [38], we deduce a closed-from solution for the target position and velocity estimation. As mentioned above, the proposed solution generally comprises two WLS steps, from which a rough WLS solution and a refined WLS solution are produced respectively.

3.1 The first WLS step

Begin by reformulating (10) as

$$r_{m,n} - R^t_m = R^r_n + \Delta r_{m,n}. \tag{17}$$

Recalling the definitions of R^t_m and R^r_n, squaring both sides of (17), and then simplifying, yield

$$2(\boldsymbol{s}^t_m - \boldsymbol{s}^r_n)^{\mathrm{T}}\boldsymbol{u} + 2r_{m,n}R^t_m = \\ r^2_{m,n} + (\boldsymbol{s}^t_m)^{\mathrm{T}}\boldsymbol{s}^t_m - (\boldsymbol{s}^r_n)^{\mathrm{T}}\boldsymbol{s}^r_n - 2R^r_n\Delta r_{m,n} \tag{18}$$

where the second-order noise term has been neglected.

By taking the derivative of (18) versus time, we establish a relation between the measurement Doppler shift and the parameter target location as follows:

$$2(\dot{\boldsymbol{s}}^t_m - \dot{\boldsymbol{s}}^r_n)^{\mathrm{T}}\boldsymbol{u} + 2(\boldsymbol{s}^t_m - \boldsymbol{s}^r_n)^{\mathrm{T}}\dot{\boldsymbol{u}} + 2\dot{r}_{m,n}R^t_m + 2r_{m,n}\dot{R}^t_m = \\ 2r_{m,n}\dot{r}_{m,n} + 2(\boldsymbol{s}^t_m)^{\mathrm{T}}\dot{\boldsymbol{s}}^t_m - 2(\boldsymbol{s}^r_n)^{\mathrm{T}}\dot{\boldsymbol{s}}^r_n - \\ 2\dot{R}^r_n\Delta r_{m,n} - 2R^r_n\Delta\dot{r}_{m,n}. \tag{19}$$

Further, taking the time derivative of (19) yields a relation between the measurement Doppler rate and the parameter target location as follows:

$$4(\dot{\boldsymbol{s}}^t_m - \dot{\boldsymbol{s}}^r_n)^{\mathrm{T}}\dot{\boldsymbol{u}} + 2\ddot{r}_{m,n}R^t_m + 4\dot{r}_{m,n}\dot{R}^t_m + 2r_{m,n}\ddot{R}^t_m = \\ 2\dot{r}_{m,n}\dot{r}_{m,n} + 2r_{m,n}\ddot{r}_{m,n} + 2(\dot{\boldsymbol{s}}^t_m)^{\mathrm{T}}\dot{\boldsymbol{s}}^t_m - 2(\dot{\boldsymbol{s}}^r_n)^{\mathrm{T}}\dot{\boldsymbol{s}}^r_n - \\ 2\ddot{R}^r_n\Delta r_{m,n} - 4\dot{R}^r_n\Delta\dot{r}_{m,n} - 2R^r_n\Delta\ddot{r}_{m,n}. \tag{20}$$

Define an auxiliary vector as

$$\boldsymbol{\theta}_1 = [\boldsymbol{u}^{\mathrm{T}}, R^t_1, R^t_2, \dots, R^t_M, \dot{\boldsymbol{u}}^{\mathrm{T}}, \dot{R}^t_1, \dot{R}^t_2, \dots, \dot{R}^t_M, \\ \ddot{R}^t_1, \ddot{R}^t_2, \dots, \ddot{R}^t_M]^{\mathrm{T}} \tag{21}$$

where $R^t_1, R^t_2, \dots, R^t_M, \dot{R}^t_1, \dot{R}^t_2, \dots, \dot{R}^t_M, \ddot{R}^t_1, \ddot{R}^t_2, \dots, \ddot{R}^t_M$ are the introduced additional variables. By stacking (18), (19) and (20) for $m = 1, 2, \dots, M$ and $n = 1, 2, \dots, N$, we can compactly recast the pseudolinear equations extracted from measurements of time delay, Doppler shift and Doppler rate as

$$\boldsymbol{G}_1\boldsymbol{\theta}_1 = \boldsymbol{h}_1 + \Delta\boldsymbol{h}_1 \tag{22}$$

and $\boldsymbol{G}_1$, $\boldsymbol{h}_1$ and $\Delta\boldsymbol{h}_1$ are expressed in submatrix as

$$\boldsymbol{G}_1=\begin{bmatrix}2\boldsymbol{G}_{1s} & 2\boldsymbol{G}_{1r} & \mathbf{0} & \mathbf{0} & \mathbf{0}\\ 2\boldsymbol{G}_{1\dot{s}} & 2\boldsymbol{G}_{1\dot{r}} & 2\boldsymbol{G}_{1s} & 2\boldsymbol{G}_{1r} & \mathbf{0}\\ \mathbf{0} & 2\boldsymbol{G}_{1\ddot{r}} & 4\boldsymbol{G}_{1\dot{s}} & 4\boldsymbol{G}_{1\dot{r}} & 2\boldsymbol{G}_{1r}\end{bmatrix}, \quad (23)$$

$$\boldsymbol{h}_1=\begin{bmatrix}\boldsymbol{h}_{1r}\\ \boldsymbol{h}_{1\dot{r}}\\ \boldsymbol{h}_{1\ddot{r}}\end{bmatrix} \quad (24)$$

where

$$\boldsymbol{G}_{1s}=\begin{bmatrix}\boldsymbol{s}_1\\ \boldsymbol{s}_2\\ \vdots\\ \boldsymbol{s}_M\end{bmatrix},\quad \boldsymbol{s}_m=\begin{bmatrix}(\boldsymbol{s}_m^t-\boldsymbol{s}_1^r)^{\mathrm{T}}\\ (\boldsymbol{s}_m^t-\boldsymbol{s}_2^r)^{\mathrm{T}}\\ \vdots\\ (\boldsymbol{s}_m^t-\boldsymbol{s}_N^r)^{\mathrm{T}}\end{bmatrix},\quad \boldsymbol{G}_{1r}=\begin{bmatrix}\boldsymbol{r}_1 & \mathbf{0}_{N\times1} & \cdots & \mathbf{0}_{N\times1}\\ \mathbf{0}_{N\times1} & \boldsymbol{r}_2 & \cdots & \mathbf{0}_{N\times1}\\ \vdots & \vdots & \ddots & \vdots\\ \mathbf{0}_{N\times1} & \mathbf{0}_{N\times1} & \cdots & \boldsymbol{r}_M\end{bmatrix},\quad \boldsymbol{r}_m=\begin{bmatrix}r_{m,1}\\ r_{m,2}\\ \vdots\\ r_{m,N}\end{bmatrix},$$

$$\boldsymbol{G}_{1\dot{s}}=\begin{bmatrix}\dot{\boldsymbol{s}}_1\\ \dot{\boldsymbol{s}}_2\\ \vdots\\ \dot{\boldsymbol{s}}_M\end{bmatrix},\quad \dot{\boldsymbol{s}}_m=\begin{bmatrix}(\dot{\boldsymbol{s}}_m^t-\dot{\boldsymbol{s}}_1^r)^{\mathrm{T}}\\ (\dot{\boldsymbol{s}}_m^t-\dot{\boldsymbol{s}}_2^r)^{\mathrm{T}}\\ \vdots\\ (\dot{\boldsymbol{s}}_m^t-\dot{\boldsymbol{s}}_N^r)^{\mathrm{T}}\end{bmatrix},\quad \boldsymbol{G}_{1\dot{r}}=\begin{bmatrix}\dot{\boldsymbol{r}}_1 & \mathbf{0}_{N\times1} & \cdots & \mathbf{0}_{N\times1}\\ \mathbf{0}_{N\times1} & \dot{\boldsymbol{r}}_2 & \cdots & \mathbf{0}_{N\times1}\\ \vdots & \vdots & \ddots & \vdots\\ \mathbf{0}_{N\times1} & \mathbf{0}_{N\times1} & \cdots & \dot{\boldsymbol{r}}_M\end{bmatrix},\quad \dot{\boldsymbol{r}}_m=\begin{bmatrix}\dot{r}_{m,1}\\ \dot{r}_{m,2}\\ \vdots\\ \dot{r}_{m,N}\end{bmatrix},$$

$$\boldsymbol{h}_{1r}=\begin{bmatrix}\boldsymbol{h}_{1r1}\\ \boldsymbol{h}_{1r2}\\ \vdots\\ \boldsymbol{h}_{1rM}\end{bmatrix},\quad \boldsymbol{h}_{1rm}=\begin{bmatrix}r_{m,1}^2+(\boldsymbol{s}_m^t)^{\mathrm{T}}\boldsymbol{s}_m^t-(\boldsymbol{s}_1^r)^{\mathrm{T}}\boldsymbol{s}_1^r\\ r_{m,2}^2+(\boldsymbol{s}_m^t)^{\mathrm{T}}\boldsymbol{s}_m^t-(\boldsymbol{s}_2^r)^{\mathrm{T}}\boldsymbol{s}_2^r\\ \vdots\\ r_{m,N}^2+(\boldsymbol{s}_m^t)^{\mathrm{T}}\boldsymbol{s}_m^t-(\boldsymbol{s}_N^r)^{\mathrm{T}}\boldsymbol{s}_N^r\end{bmatrix},\quad \boldsymbol{h}_{1\dot{r}}=\begin{bmatrix}\boldsymbol{h}_{1\dot{r}1}\\ \boldsymbol{h}_{1\dot{r}2}\\ \vdots\\ \boldsymbol{h}_{1\dot{r}M}\end{bmatrix},$$

$$\boldsymbol{h}_{1\dot{r}m}=2\begin{bmatrix}r_{m,1}\dot{r}_{m,1}+(\boldsymbol{s}_m^t)^{\mathrm{T}}\dot{\boldsymbol{s}}_m^t-(\boldsymbol{s}_1^r)^{\mathrm{T}}\dot{\boldsymbol{s}}_1^r\\ r_{m,2}\dot{r}_{m,2}+(\boldsymbol{s}_m^t)^{\mathrm{T}}\dot{\boldsymbol{s}}_m^t-(\boldsymbol{s}_2^r)^{\mathrm{T}}\dot{\boldsymbol{s}}_2^r\\ \vdots\\ r_{m,N}\dot{r}_{m,N}+(\boldsymbol{s}_m^t)^{\mathrm{T}}\dot{\boldsymbol{s}}_m^t-(\boldsymbol{s}_N^r)^{\mathrm{T}}\dot{\boldsymbol{s}}_N^r\end{bmatrix},\quad \boldsymbol{h}_{1\ddot{r}}=\begin{bmatrix}\boldsymbol{h}_{1\ddot{r}1}\\ \boldsymbol{h}_{1\ddot{r}2}\\ \vdots\\ \boldsymbol{h}_{1\ddot{r}M}\end{bmatrix},$$

$$\boldsymbol{h}_{1\ddot{r}m}=2\begin{bmatrix}\dot{r}_{m,1}\dot{r}_{m,1}+r_{m,1}\ddot{r}_{m,1}+(\dot{\boldsymbol{s}}_m^t)^{\mathrm{T}}\dot{\boldsymbol{s}}_m^t-(\dot{\boldsymbol{s}}_1^r)^{\mathrm{T}}\dot{\boldsymbol{s}}_1^r\\ \dot{r}_{m,2}\dot{r}_{m,2}+r_{m,2}\ddot{r}_{m,2}+(\dot{\boldsymbol{s}}_m^t)^{\mathrm{T}}\dot{\boldsymbol{s}}_m^t-(\dot{\boldsymbol{s}}_2^r)^{\mathrm{T}}\dot{\boldsymbol{s}}_2^r\\ \vdots\\ \dot{r}_{m,N}\dot{r}_{m,N}+r_{m,N}\ddot{r}_{m,N}+(\dot{\boldsymbol{s}}_m^t)^{\mathrm{T}}\dot{\boldsymbol{s}}_m^t-(\dot{\boldsymbol{s}}_N^r)^{\mathrm{T}}\dot{\boldsymbol{s}}_N^r\end{bmatrix}.$$

The corresponding composite noise vector $\Delta\boldsymbol{h}_1$ is given by

$$\Delta\boldsymbol{h}_1=\boldsymbol{B}_1\Delta\boldsymbol{\alpha} \quad (25)$$

where $\boldsymbol{B}_1$ is expressed in the submatrix form as

$$\boldsymbol{B}_1=\begin{bmatrix}2\boldsymbol{B} & \mathbf{0}_{MN\times MN} & \mathbf{0}_{MN\times MN}\\ 2\dot{\boldsymbol{B}} & 2\boldsymbol{B} & \mathbf{0}_{MN\times MN}\\ 2\ddot{\mathrm{B}} & 4\dot{\boldsymbol{B}} & 2\boldsymbol{B}\end{bmatrix}, \quad (26)$$

and $\boldsymbol{B}$, $\dot{\boldsymbol{B}}$ and $\ddot{\boldsymbol{B}}$ are block diagonal matrices, i.e.,

$$\boldsymbol{B}=\mathrm{diag}(\boldsymbol{B}_{11},\boldsymbol{B}_{12},\dots,\boldsymbol{B}_{1M}),$$

$$\dot{\boldsymbol{B}}=\mathrm{diag}(\dot{\boldsymbol{B}}_{11},\dot{\boldsymbol{B}}_{12},\dots,\dot{\boldsymbol{B}}_{1M}),$$

$$\ddot{\boldsymbol{B}}=\mathrm{diag}(\ddot{\boldsymbol{B}}_{11},\ddot{\boldsymbol{B}}_{12},\dots,\ddot{\boldsymbol{B}}_{1M}),$$

with

$$\boldsymbol{B}_{1m}=-\mathrm{diag}\{R_1^r,R_2^r,\dots,R_N^r\},$$

$$\dot{\boldsymbol{B}}_{1m}=-\mathrm{diag}\{\dot{R}_1^r,\dot{R}_2^r,\dots,\dot{R}_N^r\},$$

$$\ddot{\boldsymbol{B}}_{1m}=-\mathrm{diag}\{\ddot{R}_1^r,\ddot{R}_2^r,\dots,\ddot{R}_N^r\}.$$

From (22), an estimate of $\boldsymbol{\theta}_1$ is given, based on the weighted least squares minimization, as

$$\widehat{\boldsymbol{\theta}}_1=(\boldsymbol{G}_1^{\mathrm{T}}\boldsymbol{W}_1\boldsymbol{G}_1)^{-1}\boldsymbol{G}_1^{\mathrm{T}}\boldsymbol{W}_1\boldsymbol{h}_1 \quad (27)$$

where $\boldsymbol{W}_1$ is the weighting matrix determined by

$$\boldsymbol{W}_1=[\mathrm{E}(\Delta\boldsymbol{h}_1\Delta\boldsymbol{h}_1^{\mathrm{T}})]^{-1}=[\boldsymbol{B}_1\boldsymbol{Q}\boldsymbol{B}_1^{\mathrm{T}}]^{-1}. \quad (28)$$

Troublingly, as indicated in (28), $\boldsymbol{W}_1$ is a matrix related to the unknown target location. Toward this end, we turn to iteratively updating values of $\boldsymbol{W}_1$. To be more specific, by setting $\boldsymbol{W}_1=\boldsymbol{I}_{3MN\times3MN}$, we find an initial estimate of $\boldsymbol{\theta}_1$ using (27). Based on this, a better weighting matrix $\boldsymbol{W}_1$ can be formed by substituting the estimated $\boldsymbol{\theta}_1$ into (28). Then, a more accurate estimate of $\boldsymbol{\theta}_1$ is acquired by using the formed weighting matrix $\boldsymbol{W}_1$. Usually, repeating the computation of $\boldsymbol{\theta}_1$ and $\boldsymbol{W}_1$ one to two times is enough to achieve an acceptably accurate estimate.

Subtracting both sides of (27) by the true value $\boldsymbol{\theta}_1=$

$(\boldsymbol{G}_1^{\mathrm{T}}\boldsymbol{W}_1\boldsymbol{G}_1)^{-1}\boldsymbol{G}_1^{\mathrm{T}}\boldsymbol{W}_1\boldsymbol{G}_1\boldsymbol{\theta}_1$ gives rise to

$$\Delta\boldsymbol{\theta}_1 = (\boldsymbol{G}_1^{\mathrm{T}}\boldsymbol{W}_1\boldsymbol{G}_1)^{-1}\boldsymbol{G}_1^{\mathrm{T}}\boldsymbol{W}_1\Delta\boldsymbol{h}_1. \tag{29}$$

Suppose the measurement noise in $\boldsymbol{G}_1$ and $\boldsymbol{B}_1$ is small enough to be neglected. Then, taking expectation on (29) and invoking the fact that $\mathrm{E}\{\Delta\boldsymbol{\alpha}\} = \mathbf{0}_{3MN\times 1}$ yield $\mathrm{E}\{\Delta\boldsymbol{\theta}_1\} \simeq \mathbf{0}_{(3M+6)\times 1}$, which indicates the unbiasedness over a small noise region. Accordingly, the covariance (as well as the mean square error) is given, by multiplying (29) with its transpose and taking expectation, as

$$\mathrm{Cov}(\boldsymbol{\theta}_1) = (\boldsymbol{G}_1^{\mathrm{T}}\boldsymbol{W}_1\boldsymbol{G}_1)^{-1}. \tag{30}$$

3.2 The second WLS step

Observe that, in the first WLS step, to rearrange the nonlinear measurement equations into linear forms, we have introduced extra additional variables $R_1^t, R_2^t, \dots, R_M^t, \dot{R}_1^t, \dot{R}_2^t, \dots, \dot{R}_M^t, \ddot{R}_1^t, \ddot{R}_2^t, \dots, \ddot{R}_M^t$, which are functions of the target position and velocity as seen in (1), (2) and (3). Following the basic idea of two-step WLS, the second WLS step exploits these functional relations to upgrade the localization accuracy.

Toward this end, begin by letting $\widehat{\boldsymbol{u}}$, $\widehat{\dot{\boldsymbol{u}}}$, $\widehat{R}_m^t$, $\widehat{\dot{R}}_m^t$ and $\widehat{\ddot{R}}_m^t$ be the estimates of $\boldsymbol{u}$, $\dot{\boldsymbol{u}}$, R_m^t, $\dot{R}_m^t$ and $\ddot{R}_m^t$ obtained in the first WLS step, and $\Delta\boldsymbol{u}$, $\Delta\dot{\boldsymbol{u}}$, ΔR_m^t, $\Delta\dot{R}_m^t$ and $\Delta\ddot{R}_m^t$ be the corresponding estimation errors. First of all, the final target position and velocity estimate should maintain as close as possible to the target location values obtained in the first WLS step by minimizing the errors of the following equations:

$$\boldsymbol{u} = \widehat{\boldsymbol{u}} - \Delta\boldsymbol{u}, \tag{31}$$

$$\dot{\boldsymbol{u}} = \widehat{\dot{\boldsymbol{u}}} - \Delta\dot{\boldsymbol{u}}. \tag{32}$$

Meanwhile, to exploit the functional relations between additional variables and target location parameters to refine the estimate, reformulate (1), (2) and (3), respectively, as

$$2(\boldsymbol{s}_m^t)^{\mathrm{T}}\boldsymbol{u} = \boldsymbol{u}^{\mathrm{T}}\boldsymbol{u} - (R_m^t)^2 + (\boldsymbol{s}_m^t)^{\mathrm{T}}\boldsymbol{s}_m^t, \tag{33}$$

$$(\dot{\boldsymbol{s}}_m^t)^{\mathrm{T}}\boldsymbol{u} + (\boldsymbol{s}_m^t)^{\mathrm{T}}\dot{\boldsymbol{u}} = \boldsymbol{u}^{\mathrm{T}}\dot{\boldsymbol{u}} - R_m^t\dot{R}_m^t + (\boldsymbol{s}_m^t)^{\mathrm{T}}\dot{\boldsymbol{s}}_m^t, \tag{34}$$

$$2(\dot{\boldsymbol{s}}_m^t)^{\mathrm{T}}\boldsymbol{u} = \dot{\boldsymbol{u}}^{\mathrm{T}}\dot{\boldsymbol{u}} + (\dot{\boldsymbol{s}}_m^t)^{\mathrm{T}}\dot{\boldsymbol{s}}_m^t - (\dot{R}_m^t)^2 - R_m^t\ddot{R}_m^t. \tag{35}$$

Inserting $\boldsymbol{u} = \widehat{\boldsymbol{u}} - \Delta\boldsymbol{u}$, $\dot{\boldsymbol{u}} = \widehat{\dot{\boldsymbol{u}}} - \Delta\dot{\boldsymbol{u}}$, $R_m^t = \widehat{R}_m^t - \Delta R_m^t$, $\dot{R}_m^t = \widehat{\dot{R}}_m^t - \Delta\dot{R}_m^t$ and $\ddot{R}_m^t = \widehat{\ddot{R}}_m^t - \Delta\ddot{R}_m^t$, into the right side of (33), (34) and (35), and retaining only the linear error terms, lead to

$$2(\boldsymbol{s}_m^t)^{\mathrm{T}}\boldsymbol{u} = \widehat{\boldsymbol{u}}^{\mathrm{T}}\widehat{\boldsymbol{u}} - (\widehat{R}_m^t)^2 + (\boldsymbol{s}_m^t)^{\mathrm{T}}\boldsymbol{s}_m^t - 2\widehat{\boldsymbol{u}}^{\mathrm{T}}\Delta\boldsymbol{u} + 2\widehat{R}_m^t\Delta R_m^t, \tag{36}$$

$$(\dot{\boldsymbol{s}}_m^t)^{\mathrm{T}}\boldsymbol{u} + (\boldsymbol{s}_m^t)^{\mathrm{T}}\dot{\boldsymbol{u}} = \widehat{\boldsymbol{u}}^{\mathrm{T}}\widehat{\dot{\boldsymbol{u}}} - \widehat{R}_m^t\widehat{\dot{R}}_m^t + (\boldsymbol{s}_m^t)^{\mathrm{T}}\dot{\boldsymbol{s}}_m^t - \widehat{\dot{\boldsymbol{u}}}^{\mathrm{T}}\Delta\boldsymbol{u} + \widehat{\dot{R}}_m^t\Delta R_m^t - \widehat{\boldsymbol{u}}^{\mathrm{T}}\Delta\dot{\boldsymbol{u}} + \widehat{R}_m^t\Delta\dot{R}_m^t, \tag{37}$$

$$2(\dot{\boldsymbol{s}}_m^t)^{\mathrm{T}}\boldsymbol{u} = \widehat{\dot{\boldsymbol{u}}}^{\mathrm{T}}\widehat{\dot{\boldsymbol{u}}} + (\dot{\boldsymbol{s}}_m^t)^{\mathrm{T}}\dot{\boldsymbol{s}}_m^t - (\widehat{\dot{R}}_m^t)^2 - \widehat{R}_m^t\widehat{\ddot{R}}_m^t + \widehat{\ddot{R}}_m^t\Delta R_m^t - 2\widehat{\dot{\boldsymbol{u}}}^{\mathrm{T}}\Delta\dot{\boldsymbol{u}} + 2\widehat{\dot{R}}_m^t\Delta\dot{R}_m^t + \widehat{R}_m^t\Delta\ddot{R}_m^t. \tag{38}$$

Now, the final target position and velocity estimate should also minimize the equation errors in (36), (37) and (38). Therefore, defining $\boldsymbol{\theta}_2 = [\boldsymbol{u}^{\mathrm{T}}, \dot{\boldsymbol{u}}^{\mathrm{T}}]^{\mathrm{T}}$ and combining (31), (32) and (36), (37), (38), another integrated linear equation is established in the matrix form as

$$\boldsymbol{G}_2\boldsymbol{\theta}_2 = \boldsymbol{h}_2 + \Delta\boldsymbol{h}_2 \tag{39}$$

where

$$\boldsymbol{G}_2 = \begin{bmatrix} \boldsymbol{G}_{2r} \\ \boldsymbol{G}_{2\dot{r}} \\ \boldsymbol{G}_{2\ddot{r}} \end{bmatrix}, \quad \boldsymbol{G}_{2r} = \begin{bmatrix} \boldsymbol{I}_{3\times 3} & \mathbf{0}_{3\times 3} \\ 2(\boldsymbol{s}_1^t)^{\mathrm{T}} & \mathbf{0}_{3\times 1}^{\mathrm{T}} \\ 2(\boldsymbol{s}_2^t)^{\mathrm{T}} & \mathbf{0}_{3\times 1}^{\mathrm{T}} \\ \vdots & \vdots \\ 2(\boldsymbol{s}_M^t)^{\mathrm{T}} & \mathbf{0}_{3\times 1}^{\mathrm{T}} \end{bmatrix},$$

$$\boldsymbol{G}_{2\dot{r}} = \begin{bmatrix} \mathbf{0}_{3\times 3} & \boldsymbol{I}_{3\times 3} \\ 2(\dot{\boldsymbol{s}}_1^t)^{\mathrm{T}} & 2(\boldsymbol{s}_1^t)^{\mathrm{T}} \\ 2(\dot{\boldsymbol{s}}_2^t)^{\mathrm{T}} & 2(\boldsymbol{s}_2^t)^{\mathrm{T}} \\ \vdots & \vdots \\ 2(\dot{\boldsymbol{s}}_M^t)^{\mathrm{T}} & 2(\boldsymbol{s}_M^t)^{\mathrm{T}} \end{bmatrix},$$

$$\boldsymbol{G}_{2\ddot{r}} = \begin{bmatrix} 2(\dot{\boldsymbol{s}}_1^t)^{\mathrm{T}} & \mathbf{0}_{3\times 1}^{\mathrm{T}} \\ 2(\dot{\boldsymbol{s}}_2^t)^{\mathrm{T}} & \mathbf{0}_{3\times 1}^{\mathrm{T}} \\ \vdots & \vdots \\ 2(\dot{\boldsymbol{s}}_M^t)^{\mathrm{T}} & \mathbf{0}_{3\times 1}^{\mathrm{T}} \end{bmatrix},$$

$$\boldsymbol{h}_2 = \begin{bmatrix} \boldsymbol{h}_{2r} \\ \boldsymbol{h}_{2\dot{r}} \\ \boldsymbol{h}_{2\ddot{r}} \end{bmatrix}, \quad \boldsymbol{h}_{2r} = \begin{bmatrix} \widehat{\boldsymbol{u}} \\ \widehat{\boldsymbol{u}}^{\mathrm{T}}\widehat{\boldsymbol{u}} - (\widehat{R}_1^t)^2 + (\boldsymbol{s}_1^t)^{\mathrm{T}}\boldsymbol{s}_1^t \\ \widehat{\boldsymbol{u}}^{\mathrm{T}}\widehat{\boldsymbol{u}} - (\widehat{R}_2^t)^2 + (\boldsymbol{s}_2^t)^{\mathrm{T}}\boldsymbol{s}_2^t \\ \vdots \\ \widehat{\boldsymbol{u}}^{\mathrm{T}}\widehat{\boldsymbol{u}} - (\widehat{R}_M^t)^2 + (\boldsymbol{s}_M^t)^{\mathrm{T}}\boldsymbol{s}_M^t \end{bmatrix},$$

$$\boldsymbol{h}_{2\dot{r}} = \begin{bmatrix} \widehat{\dot{\boldsymbol{u}}} \\ \widehat{\boldsymbol{u}}^{\mathrm{T}}\widehat{\dot{\boldsymbol{u}}} - \widehat{R}_1^t\widehat{\dot{R}}_1^t + (\boldsymbol{s}_1^t)^{\mathrm{T}}\dot{\boldsymbol{s}}_1^t \\ \widehat{\boldsymbol{u}}^{\mathrm{T}}\widehat{\dot{\boldsymbol{u}}} - \widehat{R}_2^t\widehat{\dot{R}}_2^t + (\boldsymbol{s}_2^t)^{\mathrm{T}}\dot{\boldsymbol{s}}_2^t \\ \vdots \\ \widehat{\boldsymbol{u}}^{\mathrm{T}}\widehat{\dot{\boldsymbol{u}}} - \widehat{R}_M^t\widehat{\dot{R}}_M^t + (\boldsymbol{s}_M^t)^{\mathrm{T}}\dot{\boldsymbol{s}}_M^t \end{bmatrix},$$

$$\boldsymbol{h}_{2\ddot{r}} = \begin{bmatrix} \widehat{\dot{\boldsymbol{u}}}^{\mathrm{T}}\widehat{\dot{\boldsymbol{u}}} + (\dot{\boldsymbol{s}}_1^t)^{\mathrm{T}}\dot{\boldsymbol{s}}_1^t - (\widehat{\dot{R}}_1^t)^2 - \widehat{R}_1^t\widehat{\ddot{R}}_1^t \\ \widehat{\dot{\boldsymbol{u}}}^{\mathrm{T}}\widehat{\dot{\boldsymbol{u}}} + (\dot{\boldsymbol{s}}_2^t)^{\mathrm{T}}\dot{\boldsymbol{s}}_2^t - (\widehat{\dot{R}}_2^t)^2 - \widehat{R}_2^t\widehat{\ddot{R}}_2^t \\ \vdots \\ \widehat{\dot{\boldsymbol{u}}}^{\mathrm{T}}\widehat{\dot{\boldsymbol{u}}} + (\dot{\boldsymbol{s}}_M^t)^{\mathrm{T}}\dot{\boldsymbol{s}}_M^t - (\widehat{\dot{R}}_M^t)^2 - \widehat{R}_M^t\widehat{\ddot{R}}_M^t \end{bmatrix}.$$

The corresponding composite noise vector $\Delta\boldsymbol{h}_2$ is described by

$$\Delta\boldsymbol{h}_2 = \boldsymbol{B}_2\Delta\boldsymbol{\theta}_1 \tag{40}$$

where $\boldsymbol{B}_2$ is expressed in the submatrix form as

$$\boldsymbol{B}_2=\begin{bmatrix} -\boldsymbol{I}_{3\times3} & \boldsymbol{0}_{3\times M} & \boldsymbol{0}_{3\times3} & \boldsymbol{0}_{3\times M} & \boldsymbol{0}_{3\times M} \\ -2\times\boldsymbol{1}_{M\times1}\widehat{\boldsymbol{u}}^{\mathrm{T}} & 2\widetilde{\boldsymbol{B}} & \boldsymbol{0}_{M\times3} & \boldsymbol{0}_{M\times M} & \boldsymbol{0}_{M\times M} \\ \boldsymbol{0}_{3\times3} & \boldsymbol{0}_{3\times M} & -\boldsymbol{I}_{3\times3} & \boldsymbol{0}_{3\times M} & \boldsymbol{0}_{3\times M} \\ -\boldsymbol{1}_{M\times1}\widehat{\dot{\boldsymbol{u}}}^{\mathrm{T}} & \dot{\widetilde{\boldsymbol{B}}} & -\boldsymbol{1}_{M\times1}\widehat{\boldsymbol{u}}^{\mathrm{T}} & \widetilde{\boldsymbol{B}} & \boldsymbol{0}_{M\times M} \\ \boldsymbol{0}_{M\times3} & \ddot{\widetilde{\boldsymbol{B}}} & -2\times\boldsymbol{1}_{M\times1}\widehat{\dot{\boldsymbol{u}}}^{\mathrm{T}} & 2\dot{\widetilde{\boldsymbol{B}}} & \widetilde{\boldsymbol{B}} \end{bmatrix} \tag{41}$$

with

$$\widetilde{\boldsymbol{B}}=\mathrm{diag}(\widehat{R}_1^t,\widehat{R}_2^t,\dots,\widehat{R}_M^t), \tag{42}$$

$$\dot{\widetilde{\boldsymbol{B}}}=\mathrm{diag}(\widehat{\dot{R}}_1^t,\widehat{\dot{R}}_2^t,\dots,\widehat{\dot{R}}_M^t), \tag{43}$$

$$\ddot{\widetilde{\boldsymbol{B}}}=\mathrm{diag}(\widehat{\ddot{R}}_1^t,\widehat{\ddot{R}}_2^t,\dots,\widehat{\ddot{R}}_M^t). \tag{44}$$

Invoking the WLS minimization formula yields from (39):

$$\widehat{\boldsymbol{\theta}}_2=(\boldsymbol{G}_2^{\mathrm{T}}\boldsymbol{W}_2\boldsymbol{G}_2)^{-1}\boldsymbol{G}_2^{\mathrm{T}}\boldsymbol{W}_2\boldsymbol{h}_2 \tag{45}$$

where $\boldsymbol{W}_2$ is the weighting matrix given by

$$\boldsymbol{W}_2=[\mathrm{E}(\Delta\boldsymbol{h}_2\Delta\boldsymbol{h}_2^{\mathrm{T}})]^{-1}=[\boldsymbol{B}_2\mathrm{Cov}(\boldsymbol{\theta}_1)\boldsymbol{B}_2^{\mathrm{T}}]^{-1}. \tag{46}$$

4. Error analysis

The CRLB, which designates a fundamental lower bound on the variance for any unbiased estimators, usually serves as a benchmark for the performance of target localization algorithms. This section evaluates the performance of the proposed solution and compares it with the CRLB, under the small noise conditions.

4.1 Bias and covariance

Combining (45) and the fact that $\boldsymbol{\theta}_2=(\boldsymbol{G}_2^{\mathrm{T}}\boldsymbol{W}_2\boldsymbol{G}_2)^{-1}\cdot\boldsymbol{G}_2^{\mathrm{T}}\boldsymbol{W}_2\boldsymbol{G}_2\boldsymbol{\theta}_2$, we obtain the estimate bias as

$$\Delta\boldsymbol{\theta}_2=(\boldsymbol{G}_2^{\mathrm{T}}\boldsymbol{W}_2\boldsymbol{G}_2)^{-1}\boldsymbol{G}_2^{\mathrm{T}}\boldsymbol{W}_2\Delta\boldsymbol{h}_2. \tag{47}$$

Assume that the noise in $\boldsymbol{G}_2$ and $\boldsymbol{B}_2$ is small enough to be neglected. Then, taking expectation on (47) and recalling $\mathrm{E}\{\Delta\boldsymbol{\theta}_1\}\simeq\boldsymbol{0}_{(3M+6)\times1}$, result in $\mathrm{E}\{\Delta\boldsymbol{\theta}_2\}\simeq\boldsymbol{0}_{6\times1}$, which indicates the unbiasedness for a low noise level. The resulting covariance (as well as the mean square error) is determined, by multiplying (47) with its transpose and taking expectation, as

$$\mathrm{Cov}(\boldsymbol{\theta}_2)=(\boldsymbol{G}_2^{\mathrm{T}}\boldsymbol{W}_2\boldsymbol{G}_2)^{-1}. \tag{48}$$

4.2 CRLB

To obtain the performance limit for the target localization, the CRLB is derived next. As previously mentioned, the unknown parameter vector to be estimated and the measurement vector for the CRLB evaluation are $\boldsymbol{\theta}_2=[\boldsymbol{u}^{\mathrm{T}},\dot{\boldsymbol{u}}^{\mathrm{T}}]^{\mathrm{T}}$ and $\boldsymbol{\alpha}=[\boldsymbol{r}^{\mathrm{T}},\dot{\boldsymbol{r}}^{\mathrm{T}},\ddot{\boldsymbol{r}}^{\mathrm{T}}]^{\mathrm{T}}$ respectively. From the measurement noise model described in Section 2, the logarithm of the probability density function under $\boldsymbol{\theta}_2$ (after ignoring the constant term) is of the form

$$\ln p(\boldsymbol{\alpha}|\boldsymbol{\theta}_2)=-\frac{1}{2}(\boldsymbol{\alpha}-\boldsymbol{\alpha}^o)^{\mathrm{T}}\boldsymbol{Q}^{-1}(\boldsymbol{\alpha}-\boldsymbol{\alpha}^o). \tag{49}$$

By definition, the Fisher information matrix (FIM), whose inverse yields the CRLB, is calculated as

$$\mathrm{FIM}(\boldsymbol{\theta}_2)=\mathrm{E}\left[\frac{\partial\ln p(\boldsymbol{\alpha}|\boldsymbol{\theta}_2)}{\partial\boldsymbol{\theta}_2}\left(\frac{\partial\ln p(\boldsymbol{\alpha}|\boldsymbol{\theta}_2)}{\partial\boldsymbol{\theta}_2}\right)^{\mathrm{T}}\right]= \left(\frac{\partial\boldsymbol{\alpha}}{\partial\boldsymbol{\theta}_2}\right)^{\mathrm{T}}\boldsymbol{Q}^{-1}\left(\frac{\partial\boldsymbol{\alpha}}{\partial\boldsymbol{\theta}_2}\right) \tag{50}$$

where $\dfrac{\partial\boldsymbol{\alpha}}{\partial\boldsymbol{\theta}_2}$ is the partial derivative with respect to target location parameters and can be written into submatrices form as

$$\frac{\partial\boldsymbol{\alpha}}{\partial\boldsymbol{\theta}_2}=\begin{bmatrix} \dfrac{\partial\boldsymbol{r}}{\partial\boldsymbol{u}} & \dfrac{\partial\boldsymbol{r}}{\partial\dot{\boldsymbol{u}}} \\ \dfrac{\partial\dot{\boldsymbol{r}}}{\partial\boldsymbol{u}} & \dfrac{\partial\dot{\boldsymbol{r}}}{\partial\dot{\boldsymbol{u}}} \\ \dfrac{\partial\ddot{\boldsymbol{r}}}{\partial\boldsymbol{u}} & \dfrac{\partial\ddot{\boldsymbol{r}}}{\partial\dot{\boldsymbol{u}}} \end{bmatrix}. \tag{51}$$

Recalling the parametric form of the true measurement vector with respect to target location parameters given in (7), (8) and (9), the entries of submatrices are given as

$$\frac{\partial\boldsymbol{r}}{\partial\boldsymbol{u}}((m-1)N+n,1:3)=\frac{(\boldsymbol{u}-\boldsymbol{s}_m^t)^{\mathrm{T}}}{R_m^t}+\frac{(\boldsymbol{u}-\boldsymbol{s}_n^r)^{\mathrm{T}}}{R_n^r},$$

$$\frac{\partial\dot{\boldsymbol{r}}}{\partial\boldsymbol{u}}((m-1)N+n,1:3)=\frac{(\dot{\boldsymbol{u}}-\dot{\boldsymbol{s}}_m^t)^{\mathrm{T}}}{R_m^t}-\frac{(\boldsymbol{u}-\boldsymbol{s}_m^t)^{\mathrm{T}}\dot{R}_m^t}{(R_m^t)^2}+\frac{(\dot{\boldsymbol{u}}-\dot{\boldsymbol{s}}_n^r)^{\mathrm{T}}}{R_n^r}-\frac{(\boldsymbol{u}-\boldsymbol{s}_n^r)^{\mathrm{T}}\dot{R}_n^r}{(R_n^r)^2},$$

$$\frac{\partial\dot{\boldsymbol{r}}}{\partial\dot{\boldsymbol{u}}}((m-1)N+n,1:3)=\frac{(\boldsymbol{u}-\boldsymbol{s}_m^t)^{\mathrm{T}}}{R_m^t}+\frac{(\boldsymbol{u}-\boldsymbol{s}_n^r)^{\mathrm{T}}}{R_n^r},$$

$$\frac{\partial\ddot{\boldsymbol{r}}}{\partial\boldsymbol{u}}((m-1)N+n,1:3)=-\frac{2(\dot{\boldsymbol{u}}-\dot{\boldsymbol{s}}_m^t)^{\mathrm{T}}\dot{R}_m^t}{(R_m^t)^2}+\frac{2(\dot{R}_m^t)^2(\boldsymbol{u}-\boldsymbol{s}_m^t)^{\mathrm{T}}}{(R_m^t)^3}-\frac{\ddot{R}_m^t(\boldsymbol{u}-\boldsymbol{s}_m^t)^{\mathrm{T}}}{(R_m^t)^2}-\frac{2(\dot{\boldsymbol{u}}-\dot{\boldsymbol{s}}_n^r)^{\mathrm{T}}\dot{R}_n^r}{(R_n^r)^2}+\frac{2(\dot{R}_n^r)^2(\boldsymbol{u}-\boldsymbol{s}_n^r)^{\mathrm{T}}}{(R_n^r)^3}-\frac{\ddot{R}_n^r(\boldsymbol{u}-\boldsymbol{s}_n^r)^{\mathrm{T}}}{(R_n^r)^2},$$

$$\frac{\partial\ddot{\boldsymbol{r}}}{\partial\dot{\boldsymbol{u}}}((m-1)N+n,1:3)=\frac{2(\dot{\boldsymbol{u}}-\dot{\boldsymbol{s}}_m^t)^{\mathrm{T}}}{R_m^t}-$$

$$\frac{2(\boldsymbol{u}-\boldsymbol{s}_m^t)^{\mathrm{T}}\dot{R}_m^t}{(R_m^t)^2}+\frac{2(\dot{\boldsymbol{u}}-\dot{\boldsymbol{s}}_n^r)^{\mathrm{T}}}{R_n^r}-\frac{2(\boldsymbol{u}-\boldsymbol{s}_n^r)^{\mathrm{T}}\dot{R}_n^r}{(R_n^r)^2}$$

for $m=1,2,\dots,M; n=1,2,\dots,N$ and zero elsewhere.

Form (50), it follows that the CRLB can be given by

$$\mathrm{CRLB}(\boldsymbol{\theta}_2)=\mathrm{FIM}(\boldsymbol{\theta}_2)^{-1}. \quad (52)$$

It is not difficult to show that the CRLB in (52) and the covariance in (48) are of the same form. Not only that, under the assumptions that the measurement noises are sufficiently small, we have after some algebraic manipulations

$$\boldsymbol{G}_2 \simeq \frac{\partial \boldsymbol{\alpha}}{\partial \boldsymbol{\theta}_2}. \quad (53)$$

By now, it is reasonable to arrive at the conclusion that the covariance is approximately equivalent to the CRLB, implying that the CRLB is achieved by using the proposed solution for small measurement noises.

5. Numerical examples

In this section, numerical examples are performed to verify the theoretical development of the proposed solution. In the numerical examples, we consider a geolocation scenario as illustrated in Fig. 1, where the positions and velocities of the transmitters T_1-T_5 and receivers R_1-R_5 are enumerated in Table 1. Note that in the following simulations only three transmitters T_1-T_3 and three receivers R_1-R_3 are employed, unless otherwise specified. The position of the aircraft target is $[30\,000, -30\,000, 1\,000]^{\mathrm{T}}$ m, and it moves with a velocity of $[-500, 500, 50]^{\mathrm{T}}$ m/s.

Table 1 Position and velocity of transmitters and receivers

Station	x/m	y/m	z/m	$\dot{x}$/(m/s)	$\dot{y}$/(m/s)	$\dot{z}$/(m/s)
T_1	4 000	4 000	−250	50	50	0
T_2	4 000	−4 000	250	50	50	25
T_3	−4 000	4 000	750	50	50	50
T_4	−4 000	−4 000	500	50	50	100
T_5	10 000	5 000	100	200	100	25
R_1	0	5 000	0	200	0	0
R_2	5 000	0	500	0	200	100
R_3	0	−5 000	1 000	−200	0	200
R_4	−5 000	0	1 500	0	−200	50
R_5	0	0	0	0	0	0

Simulation results illustrate the performance of the proposed solution for different measurement noise levels [39], which can be obtained from the following equations:

$$\mathrm{Var}(r)=c^2\frac{1}{B_s^2}\frac{1}{B_nT}\frac{1}{\mathrm{SNR}}, \quad (54)$$

$$\mathrm{Var}(\dot{r})=\lambda^2\frac{3}{\pi^2T^2}\frac{1}{B_nT}\frac{1}{\mathrm{SNR}}, \quad (55)$$

$$\mathrm{Var}(\ddot{r})=\lambda^2\frac{180}{\pi^2T^4}\frac{1}{B_nT}\frac{1}{\mathrm{SNR}} \quad (56)$$

where c is the signal propagation speed, λ is the signal wavelength, B_n is the noise bandwidth, B_s is the signal bandwidth, T is the integration time. Assume that the MPR system employs digital video broadcasting (DVB) broadcasters as illuminators, and the corresponding parameters are $\lambda = 0.375$ m, $B_s = 8$ MHz, $T = 1$ s and $B_n = 20$ MHz. The SNR is related to many factors including transmit power, transmitter-to-target and target-to-receiver ranges, target bistatic radar cross-section, and so on. Combining the study in [40] and [41], we let the SNR ranges from −70 dB to −20 dB to characterize the performance of the proposed solution for different SNR levels. The root mean squared error (RMSE) and bias are employed as the performance measures, which come from 1 000 independent runs for various SNR values.

5.1 Delay – Doppler-based localization versus delay – Doppler – Doppler rate-based localization

In order to demonstrate that using the Doppler rate measurement in addition to measurements of time delay and Doppler shift provides the estimation of target position and velocity with a higher accuracy, we present and compare the CRLB of localization using delay and Doppler against localization using delay, Doppler and Doppler rate, versus various SNRs. The results are shown in Fig. 2.

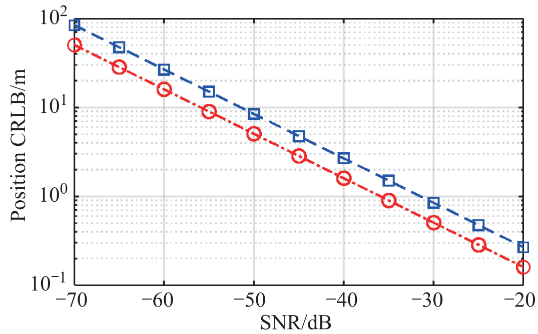

(a) Position CRLB

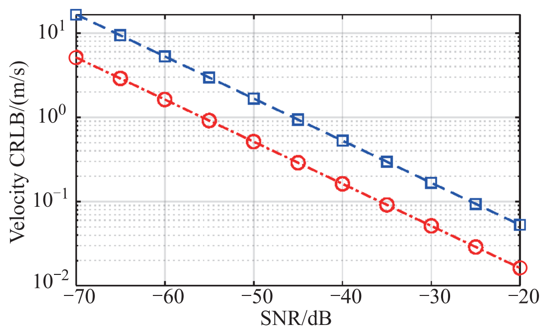

(b) Velocity CRLB

: Localization using delay and Doppler;
: Localization using delay, Doppler, and Doppler rate.

Fig. 2 CRLB comparison between delay – Doppler-based localization and delay – Doppler – Doppler rate-based localization

With the increase of SNR, both delay – Doppler-based localization and delay – Doppler – Doppler rate-based localization give better localization performance. Over the whole SNR range, the CRLB of delay – Doppler – Doppler rate-based localization is remarkably below the delay – Doppler-based localization, especially for velocity estimation. The former benefit from the additional measurement Doppler rate. This signifies the necessity of taking into account the measurement Doppler rate during the design of localization algorithms.

5.2 Evaluation of different localization methods

Next, we study the localization performance of the proposed solution in terms of RMSE and bias, as SNR varies. We also compare its performance against the Taylor-series method (with the true position and velocity as the initial guess) and the delay – Doppler localization method suggested in [32]. Moreover, the CRLB is also plotted as a benchmark. The results are illustrated in Fig. 3 and Fig. 4.

As can be seen from Fig. 3, the localization RMSE of delay – Doppler-based localization is apparently higher, compared to the family of delay – Doppler – Doppler rate-based localization methods. The excess RMSE for the delay – Doppler-based localization is of course due to the fact that it does not employ the Doppler rate measurements. Both the Taylor-series method and the proposed solution give the similar performance by attaining the CRLB at sufficiently high SNR conditions. Note that the localization problem here is highly nonlinear, and hence in practice, both the Taylor-series method and the proposed solution will suffer from the threshold phenomenon when the SNR is small enough. As analyzed, the Taylor-series method deviates from the CRLB and gives an inaccurate solution at SNR values below -50 dB, whereas the proposed solution still coincides with the CRLB at this level of SNR. Even at SNR values below -60 dB, the proposed solution is still significantly superior to the Taylor-series method, although its RMSE begins to digress from the CRLB.

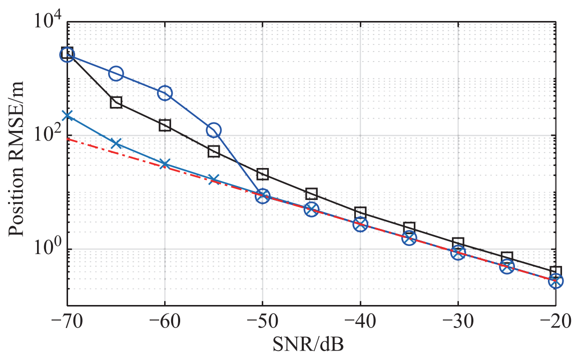

(a) Position RMSE

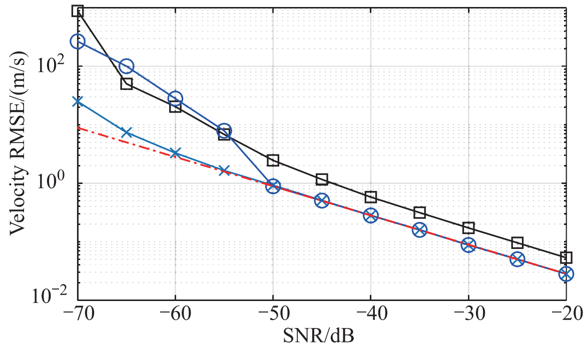

(b) Velocity RMSE

: Delay–Doppler-based localization;
: Taylor-series method;
: The proposed solution; : Root CRLB.

Fig. 3 Localization RMSE versus SNR

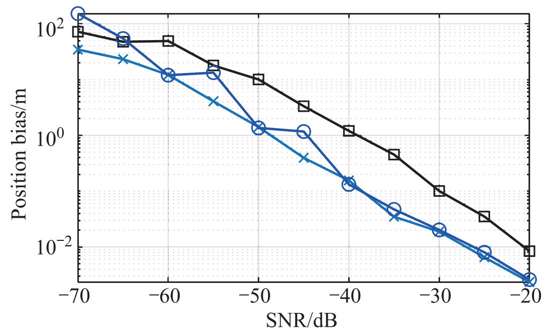

(a) Position bias

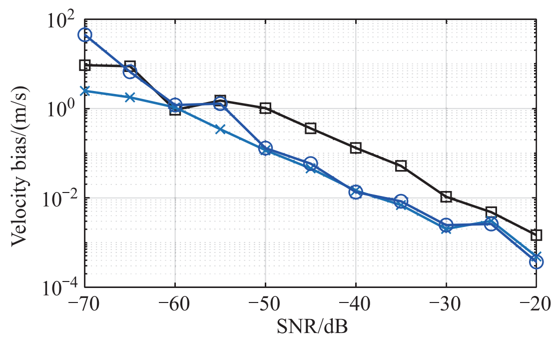

(b) Velocity bias

: Delay–Doppler-based localization;
: Taylor-series method;
: The proposed solution.

Fig. 4 Localization bias versus SNR

In terms of bias, it is clear from Fig. 4 that the proposed solution offers excellent localization performance compared with other methods. Note that as the SNR decreases, the biases of the three localization methods increase. Such findings are partially explained by the nonlinearity nature of the localization problem.

5.3 Effect of number of transmitters and receivers on performance of the proposed solution

It is intuitively reasonable that increasing the number of transmitters and receivers will improve the performance of localization methods. To numerically show the effect of the number of transmitters and receivers on the performance of the proposed solution, three cases with different numbers of transmitters and receivers are considered. We choose $M = 3$ and $N = 3$ $(T_1 - T_3, R_1 - R_3)$ for the first case, $M = 4$ and $N = 4$ $(T_1 - T_4, R_1 - R_4)$ for the second case, and $M = 3$ and $N = 3$ $(T_1 - T_5, R_1 - R_5)$ for the third case. The resulting RMSEs and biases are shown in Fig. 5 and Fig. 6.

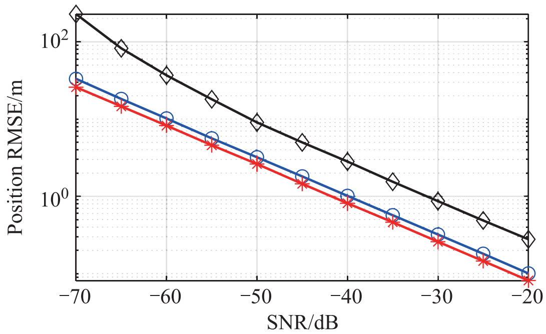

(a) Position RMSE

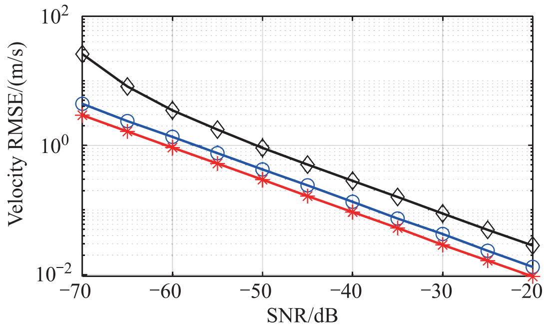

(b) Velocity RMSE

: M=3, N=3; : M=4, N=4; : M=5, N=5.

Fig. 5 Effect of number of transmitters and receivers on localization RMSE of the proposed solution

Not surprisingly, as displayed in Fig. 5 and Fig. 6, as the number of transmitters and receivers increases, the proposed solution performs better in terms of both RMSE and bias.

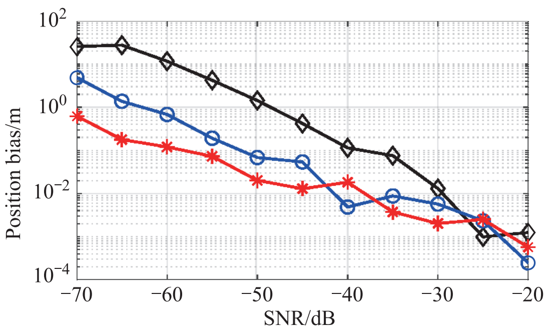

(a) Position bias

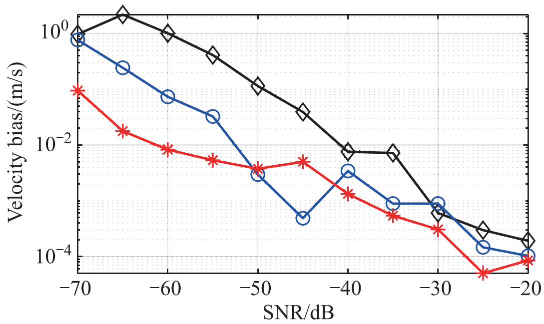

(b) Velocity bias

: M=3, N=3; : M=4, N=4; : M=5, N=5.

Fig. 6 Effect of number of transmitters and receivers on localization bias of the proposed solution

On the other hand, however, as the number of transmitters and receivers increases, the improvement rate decreases rapidly. That is to say, as the number of transmitters and receivers increases, the performance curve of the proposed solution versus SNR shows a tendency to a bound curve.

5.4 Comparison of computational cost

As mentioned above, in the proposed solution, the additional measurement Doppler rate provides the estimation of target position and velocity with a higher accuracy, but meanwhile, it certainly will require a higher computational load. To numerically evaluate the computational burden of the proposed solution, in Table 2, we enumerate and compare the time cost of the proposed solution and delay – Doppler-based localization suggested in [32]. It should be pointed out that, the time cost is obtained from the average time of 1 000 independent runs. Main configuration of the computer is CPU: Intel(R) Core (TM) i5-7200U @ 2.50 GHz; RAM: 8.00 G; Operating system: Windows 10 64 bit; Software: Matlab 2018a.

Table 2 Time cost of localization methods ms

Method	Time cost
Delay – Doppler-based localization (method in [32])	0.52
Delay – Doppler – Doppler rate-based localization (the proposed solution)	0.66

As evident in Table 2, the proposed solution costs more time than the delay – Doppler-based localization method, due to the additional measurement Doppler rate. Nevertheless, the excess time cost is not remarkable (an increase of 27%). That is to say: it is at the expense of more time cost that the proposed solution achieves a higher localization accuracy. Recalling remarkable performance improvement, the excess time cost is worthy and acceptable.

6. Conclusions

The CAF is a standard method used in passive radar, which produces time delay and Doppler shift between the echo signal and the reference signal, two most commonly used measurements in target localization. The Doppler rate, obtained from the extended CAF, makes it possible to dramatically improve the localization accuracy. This paper uses Doppler rate in addition to time delay and Doppler shift as measurements to estimate the target position and velocity. A closed-form solution is explored, by following the basic idea of two-step. The proposed closed-form solution requires no initial estimate and guarantees global convergence. Simulation results demonstrate that delay – Doppler – Doppler rate-based localization has a higher localization accuracy than delay – Doppler-based localization although the former requires higher but acceptable time cost, and the proposed solution is proved to perform better than existing methods.

References

[1] ZAIMBASHI A. Broadband target detection algorithm in FM-based passive bistatic radar systems. IET Radar, Sonar & Navigation, 2016, 10(8): 1485 – 1499.

[2] TUYSUZ B, URBINA J V, MATHEWS J D. Effects of the equatorial electrojet on FM-based passive radar systems. IEEE Trans. on Geoscience and Remote Sensing, 2017, 55(7): 4082 – 4088.

[3] SENDALL J L, MAASDORP F D V. Detection state refinement in FM multistatic passive radar. Proc. of the IEEE Radar Conference, 2017: 717 – 721.

[4] BOURNAKA G, UMMENHOFER M, CRISTALLINI D, et al. Experimental study for transmitter imperfections in DVB-T based passive radar. IEEE Trans. on Aerospace and Electronic Systems, 2018, 54(3): 1341 – 1354.

[5] BOLVARDI H, DERAKHTIAN M, SHEIKHI A. Dynamic clutter suppression and multitarget detection in a DVB-T-based passive radar. IEEE Trans. on Aerospace and Electronic Systems, 2017, 53(4): 1812 – 1825.

[6] FILIPPINI F, COLONE F, CRISTALLINI D, et al. Experimental results of polarimetric detection schemes for DVB-T-based passive radar. IET Radar, Sonar & Navigation, 2017, 11(6): 883 – 891.

[7] SCHUPBACH C, PATRY C, MAASDORP F, et al. Micro-UAV detection using DAB-based passive radar. Proc. of the IEEE Radar Conference, 2017: 1037 – 1040.

[8] SCHUPBACH C, BONIGER U. Jamming of DAB-based passive radar systems. Proc. of the European Radar Conference, 2016: 157 – 160.

[9] SHI Y F, PARK S H, SONG T L. Multitarget tracking in cluttered environment for a multistatic passive radar system under the DAB/DVB network. EURASIP Journal on Advances in Signal Processing, 2017. DOI: 10.1186/s13634-017-0445-4.

[10] BLAZQUEZ R, CASAMAYON J, BURGOS M. LTE-R based passive multistatic radar for high-speed railway network surveillance. Proc. of the European Radar Conference, 2018: 6 – 9.

[11] TAYLOR F D, LIEVSAY J R. LTE bandwidth and modulation scheme effects on passive bistatic radar. Proc. of the 52nd Asilomar Conference on Signals, Systems, and Computers, 2018: 916 – 919.

[12] BARTOLETTI S, CONTI A, WIN M Z. Passive radar via LTE signals of opportunity. Proc. of the IEEE International Conference on Communications Workshops, 2014: 181 – 185.

[13] KLOCK C, WINKLER V, EDRICH M. LTE-signal processing for passive radar air traffic surveillance. Proc. of the 18th International Radar Symposium, 2017: 1 – 9.

[14] HIGGINS T, WEBSTER T, MOKOLE E L. Passive multistatic radar experiment using WiMAX signals of opportunity, Part 1: Signal processing. IET Radar, Sonar & Navigation, 2016, 10(2): 238 – 247.

[15] WEBSTER T, HIGGINS T, MOKOLE E L. Passive multistatic radar experiment using WiMAX signals of opportunity, Part 2: Multistatic velocity backprojection. IET Radar, Sonar & Navigation, 2016, 10(2): 248 – 255.

[16] COLONE F, MARTELLI T, BONGIOANNI C, et al. WiFi-based PCL for monitoring private airfields. IEEE Aerospace and Electronic Systems Magazine, 2017, 32(2): 22 – 29.

[17] COLONE F, MARTELLI T, LOMBARDO P. Quasi-monostatic versus near forward scatter geometry in WiFi-based passive radar sensors. IEEE Sensors Journal, 2017, 17(15): 4757 – 4772.

[18] MARTELLI T, MURGIA F, COLONE F, et al. Detection and 3D localization of ultralight aircrafts and drones with a WiFi-based passive radar. Proc. of the International Conference on Radar Systems, 2017: 1 – 6.

[19] BRISKEN S, MOSCADELLI M, SEIDEL V, et al. Passive radar imaging using DVB-S2. Proc. of the IEEE Radar Conference, 2017: 552 – 556.

[20] PASTINA D, SANTI F, PIERALICE P. Maritime moving target long time integration for GNSS-based passive bistatic radar. IEEE Trans. on Aerospace and Electronic Systems, 2018, 54(6): 3060 – 3083.

[21] GRONOWSKI K, SAMCZYNSKI P, STASIAK K, et al. First results of air target detection using single channel passive radar utilizing GPS illumination. Proc. of the IEEE Radar Conference, 2019: 1 – 6.

[22] WANG D H, BAO Q L, TIAN R Q, et al. Bistatic weak target detection method using non-cooperative air surveillance radar. Journal of Systems Engineering and Electronics, 2015, 26(5): 954 – 963.

[23] OLSEN K E, ASEN W. Bridging the gap between civilian and military passive radar. IEEE Aerospace and Electronic Systems Magazine, 2017, 32(2): 4 – 12.

[24] DIMITRIOS O, PANAGIOTIS N, GEORGE L, et al. Passive radars and their use in the modern battlefield. Journal of Computations & Modelling, 2019, 9(2): 37 – 61.

[25] EDRICH M, SCHROEDER A, MEYER F. Design and performance evaluation of a mature FM/DAB/DVB-T multi-illuminator passive radar system. IET Radar, Sonar & Navigation, 2014, 8(2): 114 – 122.

[26] ZHANG X, LI H B, LIU J, et al. Joint delay and Doppler estimation for passive sensing with direct-path interference. IEEE Trans. on Signal Processing, 2016, 64(3): 630 – 640.

[27] LIU J, LI H B, HIMED B. On the performance of the cross-correlation detector for passive radar applications. Signal Processing, 2015, 113: 32 – 37.

[28] TAO R, ZHANG W Q, CHEN E Q. Two-stage method for joint time delay and Doppler shift estimation. IET Radar, Sonar & Navigation, 2008, 2(1): 71 – 77.

[29] DU Y S, WEI P. An explicit solution for target localization in noncoherent distributed MIMO radar systems. IEEE Signal Processing Letters, 2014, 21(9): 1093 – 1097.

[30] YANG H, CHUN J. An improved algebraic solution for moving target localization in noncoherent MIMO radar systems.

IEEE Trans. on Signal Processing, 2016, 64(1): 258 – 270.

[31] AMIRI R, BEHNIA F, SADR M A M. Efficient positioning in MIMO radars with widely separated antennas. IEEE Communications Letters, 2017, 21(7): 1569 – 1572.

[32] ZHAO Y S, ZHAO Y J, ZHAO C. A novel algebraic solution for moving target localization in multi-transmitter multi-receiver passive radar. Signal Processing, 2018, 143: 303 – 310.

[33] WANG H, HONG L N, YI J X, et al. A novel migration compensation algorithm for passive radar using digital TV signals. Journal of Electronics and Information Technology, 2015, 37(5): 1017 – 1022. (in Chinese)

[34] MALANOWSKI M. Detection and parameter estimation of manoeuvring targets with passive bistatic radar. IET Radar, Sonar & Navigation, 2012, 6(8): 739 – 745.

[35] GUAN X, ZHONG L H, HU D H, et al. An extended processing scheme for coherent integration and parameter estimation based on matched filtering in passive radar. Journal of Zhejiang University — Science C (Computers & Electronics), 2014, 15(11): 1071 – 1085.

[36] HU D X, HUANG Z, CHEN X, et al. A moving source localization method using TDOA, FDOA and Doppler rate measurements. IEICE Trans. on Communications, 2016, 99(3): 758 – 766.

[37] LIU Z X, HU D X, ZHAO Y S, et al. An algebraic method for moving source localization using TDOA, FDOA, and differential Doppler rate measurements with receiver location errors. EURASIP Journal on Advances in Signal Processing, 2019. DOI: 10.1186/s13634-019-0621-9.

[38] HO K C, XU W. An accurate algebraic solution for moving source location using TDOA and FDOA measurements. IEEE Trans. on Signal Processing, 2004, 52(9): 2453 – 2463.

[39] HU D X, HUANG Z, ZHANG S Y, et al. Joint TDOA, FDOA and differential Doppler rate estimation method and its performance analysis. Chinese Journal of Aeronautics, 2018, 31(1): 137 – 147.

[40] ZHENG J B, SU T, LIU H W, et al. Radar high-speed target detection based on the frequency-domain deramp-keystone transform. IEEE Journal of Selected Topics in Applied Earth Observations and Remote Sensing, 2016, 9(1): 285 – 294.

[41] ZAIMBASHI A. Target detection in analog terrestrial TV-based passive radar sensor: joint delay – Doppler estimation. IEEE Sensors Journal, 2017, 17(17): 5569 – 5580.

Biographies

ZHAO Yongsheng was born in 1990. He is currently working toward his Ph.D. degree in PLA Strategic Support Force Information Engineering University. His current research interests include multistatic passive radar, target localization, radar signal processing, estimation theory, and detection theory.
E-mail: ethanchioa@aliyun.com

HU Dexiu was born in 1983. He is a Ph.D. and a lecturer in PLA Strategic Support Force Information Engineering University. His current research interests include radar signal processing, estimation theory, and detection theory.
E-mail: paper_hdx@126.com

ZHAO Yongjun was born in 1964. He is currently a professor in PLA Strategic Support Force Information Engineering University. His current research interests include radar signal processing and array signal processing.
E-mail: zhaoyongjuntg@126.com

LIU Zhixin was born in 1991. He is currently working toward his Ph.D. degree in PLA Strategic Support Force Information Engineering University. His current research interests include DOA estimation, passive location, and satellite communication.
E-mail: liuzhixin54@sina.com